Int. J. Electrochem. Sci., 8 **(2013)** 4305 - 4327

International Journal of
ELECTROCHEMICAL
SCIENCE
www.electrochemsci.org

Quantum Chemical Studies on the Inhibiting Effect of New Synthesized Bipyrazols of C38 Steel Corrosion in 1M HCl

A. Guendouz[1], *N. Missoum*[2], *A. Chetouani*[3,4,*], *S. S. Al-Deyab*[5], *B. Ben Cheikhe*[1], *N. Boussalah*[2], *B. Hammouti*[3,5], *M. Taleb*[1], *A. Aouniti*[3]

[1] Laboratoire d'Ingénierie des Matériaux, Modélisation et Environnement, Faculté des Sciences Dhar El Mahraz, Université Allal Ben Abdellah, BP 1796, 30000 Atlas, Fès, Morocco.
[2] Laboratoire des Substances Naturelles et Bioactives (LASNABIO), BP 119, 13000 Tlemcen, Algeria
[3] Laboratoire de Chimie Appliquée et Environnement, LCAE-URAC18, COSTE, Département de Chimie, Faculté des Sciences, Université Mohamed Premier, BP 524, 60000 Oujda, Morocco
[4] Laboratoire de Chimie Physique, Centre Régionale des Métiers de l'Education et de Formation "CRMEF", de la Régionale Orientale, Morocco.
[5] Petrochemical Research Chair, Chemistry Department, College of Science, King Saud University, P.O. Box 2455, Riyadh 11451, Saudi Arabia.
[*]E-mail: ahmedchetouani70@hotmail.com

Received: 29 December 2012 / *Accepted:* 28 January 2013 / *Published:* 1 March 2013

The inhibitory activity of new synthesized and characterised bipyrazol derivatives: methyl 2- (bis[(3,5-dimethyl-1*H*-pyrazol-1-yl)methyl]amino)-4-methylpentanoate (BT39), methyl 2- (bis[(3,5-dimethyl-1*H*-pyrazol-1-yl)methyl]amino)-3-meyhylbutanoate (BT40) and methyl 2-(bis[(3,5-dimethyl-1H-pyrazol-1-yl)methyl]amino)propanoate (BT45) towards corrosion of C38 steel in molar HCl medium by weight loss and electrochemical technique shows that these compounds were very effective inhibitors, their protection percentage exceeded 88% for (BT40) at low concentrations as much as 10^{-2}M. A cathodic type of inhibition from polarization and a charge transfer mechanism from impedance study in absence and presence of these compounds were found. Langmuir adsorption isotherm is obtained. Relation between inhibition efficiency and molecular structure of (BT36), (BT43) and (BT45) is discussed by considering quantum chemical parameters. The study is completed by the density functional approach B3LYP/6-31G calculations. The quantum chemical parameters calculated show a good correlation to the inhibition efficiency. The highest occupied molecular orbital (HOMO), the lowest unoccupied molecular orbital (LUMO), the separation energy (ΔE) and the dipole moment (μ), explain well experimental data.

Keywords: bipyrazol; Inhibition; Corrosion; hydrochloric acid; quantum chemical.

1. INTRODUCTION

Chemical cleaning and pickling processes are widely used in industrial processes to remove corrosion scales from metallic surface in high concentrated acidic media at elevated temperature

between 60 and 95°C. Inhibitors are quietly required to protect metals against acid attack. Organic compounds containing electronegative functional groups and π-electron in triple or conjugated double bonds are usually goods inhibitors. Heteroatom's as sulphur, phosphorus, nitrogen and oxygen as well as aromatic ring in their structure are the major adsorption centres. Effectively the heterocyclic molecules are generally good inhibitors of corrosion of metallic materials. The remarkable inhibitory effect is related to the presence of heteroatom's such as nitrogen and oxygen in the ring which facilitates its adsorption on the metal surface following the sequence O < N [1-6]. The molecular electronic structure with number of adsorption active centres such as S, N and O atoms, the molecular size, the mode of adsorption, the formation of metallic complexes and the projected area of the inhibitor on the metallic surface (degree of surface coverage) also affect the efficiency of inhibition [7-10].

Recently more study shows that the inhibitive effect found to enhance of several organic compounds for steel in acid solutions. Heterocyclic compounds specify of the corrosion behaviour of iron and steel in acidic solutions are usually employed for their rapid action. The synthesis of new pyrazolic, bipyrazolic and tripyrazole compounds is an easy way to obtain several compounds of which the molecular structures contain several heteroatoms and several substituents. This allowed various molecules to be tested on different interfaces metal/ corrosive solution combinations and have been reported to be excellent inhibitors of iron in 1M HCl [9, 11, 12].

More work in our laboratory, realized a correlation between experimental efficiencies of inhibitors and the results of quantum chemical calculations, and constructed a composite index of some of the key quantum chemical parameters in order to characterize the inhibition performance of the tested molecules. The quantum calculations tend to correlate the effect of structural parameters of substituted pyrazolic to their inhibition efficiencies of corrosion of steel in HCl solution. Molecular orbital calculations are performed looking for good theoretical parameters to characterize the inhibition property of inhibitors, which will be helpful to gain insight into the mechanism of corrosion inhibition and then to simulate the adsorption mode of the inhibitor on the metal surface. Also, from the calculations we will try to explain which adsorption site is favoured to bind to the metal surface [13-18].

The goal of the present work is to study the inhibition of methyl 2- (bis[(3,5-dimethyl-1*H*-pyrazol-1-yl)methyl]amino)-4-methylpentanoate,(BT39), methyl 2- (bis[(3,5-dimethyl-1*H*-pyrazol-1-yl)methyl]amino)-3-meyhylbutanoate (BT40) and methyl 2-(bis[(3,5-dimethyl-1H-pyrazol-1-yl)methyl]amino)propanoate (BT45), on the C38 steel corrosion in molar hydrochloric acid. It is also aimed to predict the thermodynamic feasibility of inhibitors adsorption on metallic surface. To this end, potentiodynamic polarization curves, Tafel plot analysis and electrochemical impedance spectroscopy (EIS) were the corrosion test used in this study. Beside detailed investigation of temperature and immersion time effects was also studied and discussed to more understanding the adsorption mechanism of the studied inhibitors. The quantum calculations tend to correlate the effect of structural parameters of substituted bipyrazols to their inhibition efficiencies of corrosion of C38 steel in HCl solution. Molecular orbital calculations are performed looking for good theoretical parameters to characterize the inhibition property of inhibitors, which will be helpful to gain insight into the mechanism of corrosion inhibition and then to simulate the adsorption mode of the inhibitor on

the metal surface. Also, from the calculations we will try to explain which adsorption site is favoured to bind to the metal surface, with the substitution.

2. EXPERIMENTAL

2.1. Synthesis of the bipyrazolic compounds

In the studied, the bipyrazolic compounds are product for analysis. The Chemical structure compound is presented below in Scheme 1. The organic compounds bipyrazolic compounds tested as corrosion inhibitors were synthesized purified and characterized by 1H NMR spectra and 13C NMR spectra were recorded on a Bruker 300 (operating at 300.13 MHz for 1H, 75.47 MHz for 13C in CDCl3) spectrometer. Chemical shifts were listed in ppm and were reported relative to tetramethylsilane. The IR spectra were taken using KBr discs on Mattson Genisis FTIR. The mass spectra have been obtained on a Micro mass LCT. New functional pyrazolic derivatives (BT39), (BT40) and (BT45) were prepared respectively by condensation of two equivalents of (3,5-dimethyl - 1H -pyrazol-1-yl)methanol with one equivalent of amino acid ester hydrochloride derivatives (commercially available) in anhydrous solvents. All reactions were carried out at room temperature under stirring from 4 to 6 days and under inert atmosphere.

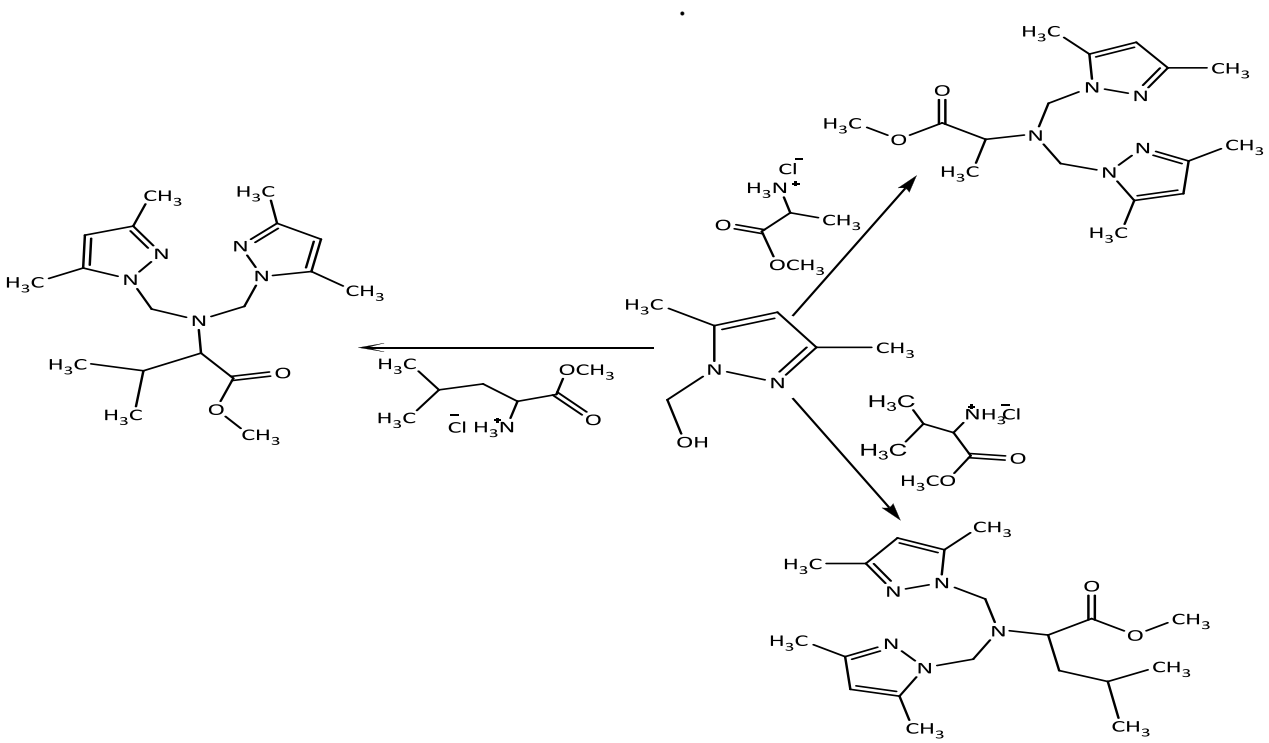

Scheme 1. Structure of tested compounds

The compounds from (BT39), (BT40) and (BT45) were already described and published. The methyl-2-(bis((3,5-dimethyl-1H-pyrazol-1-yl)methyl)amino)-3-methylbutanoate BT40: Yield: 72 %. 1HNMR(300MHz, $CDCl_3$, ı, ppm): 5.77 (s, 2H,*H*–Pz); 5.13–5.04 (dd, 4H, N–CH_2–N, J = 13.82 Hz);

3.57 (s, 3H, O–C*H*$_3$); 3.18 (d, 1H, N–C*H*–CO, J = 11.10 Hz); 2.28 (m, 1H, CH$_3$–C*H*–CH3); 2.19–2.10 (4 s, 12H, pz–C*H*$_3$); 0.83 (d, 3H, CH–C*H*$_3$, J = 6.50 Hz); 0.70 (d, 3H, CH–C*H3*, J = 6.54 Hz). 13C NMR (75 MHz, CDCl$_3$, ı, ppm): 172.66 (–*C*OO); 147.7 (N *C*–CH3); 139.91 (C = *C*–CH3); 105.62 (*C*H–pz); 70.38 (N–*C*H–COO); 67.62 (N–*C*H$_2$–N); 67.25 (N–*C*H2–N); 51.79 (O–*C*H3); 31.67 (*C*H(CH3)2); 19.67 (CH(*C*H3)2); 19.49 (CH(*C*H$_3$)$_2$); 13.6 (C–*C*H$_3$); 10.53 (C–*C*H$_3$). FTIR (KBr, cm−1): 3026–2926 (_C–H); 1731 (_C O); 1556–1461 (_C N,C C); 1200 (ıC–O); 1109 (_C–N); 780 (ıC–H). MS (ES) *m*/*z* (%) = 347.69 (70); 283.54 (84); 251.88 (100); 241.95 (10); 108.88 (5).

Methyl 2-(bis ((3, 5-dimethyl-1H-pyrazol-1-yl)methyl) amino)- 3-methylpentanoate BT39: Yield: 78 %. 1HNMR(300MHz, CDCl$_3$, ı, ppm): 5.78 (s, 2H,*H*–Pz); 5.13–5.02 (dd, 4H, N–C*H*2–N, J = 13.61 Hz); 3.63 (s, 3H, O–C*H*$_3$); 3.39 (t, 1H, N–C*H*–CO, J = 7.21 Hz); 2.18–2.05 (4 x s, 12H, pz–C*H*3); 1.36–1.68 (m, 3H, –C*H*$_2$–C*H*); 0.88 (d, 3H, –C*H*$_3$, J = 6.52 Hz); 0.54 (d, 3H, –C*H*$_3$, J = 6.32 Hz). 13C NMR (75 MHz, CDCl$_3$, ı, ppm): 173.86 (–*C*OO); 147.65 (N *C*–CH$_3$); 139.91 (C *C*–CH$_3$); 105.89 (*C*H–pz); 70.44 (N–*C*H–COO); 67.62 (N–*C*H$_2$–N); 67.25 (N–*C*H$_2$–N); 51.79 (O–*C*H$_3$); 31.67 (*C*H(CH$_3$)$_2$); 19.67 (CH(*C*H$_3$)$_2$); 19.49 (CH(*C*H$_3$)$_2$); 10.53 (C–*C*H$_3$); 13.38 (C–*C*H$_3$). FTIR (KBr, cm−1): 2954–2869 (_C–H); 1734 (_C O); 1557–1422 (_C N,C C); 1200 (ıC–O); 1129 (_C–N); 785-715 (ıC–H). MS (ES)*m*/*z* (%) = 361.70 (100); 265.89 (20); 108.87 (2.5).

For Methyl 2-(bis ((3, 5-dimethyl-1H-pyrazol-1-yl)methyl) amino)propanoate BT45: Yield : 68% *RMNH*^{1}: 5.95 (s,2H, H2), 5.05-5,21 (AB, J1=14,7Hz, J2=15,0Hz, H4+H4'); (d, CH2, J= 14.7 Hz), 3.49 (s, 3H, H7), 3.41 (q, H5), 2.57 (s,6H,H3), 2.25 (s, 6H, H1), 1.33 (d, H6, J= 7.2 Hz). *MS (Electro spray)*:319.67(45%); 255.63(100%); 223.84(90%); 213.95(20%); 108.92(12%).

The chemical formulas of bipyrazol compounds studied and the optimized molecular structures of the studied inhibitors are represented as follows in figure 1. The geometric structures of the inhibitors by optimizing of their bond lengths, bond angles and dihedral angles, table 1, are minimized by MM2 method by ChemBio3D Ultra 11.0 soft.

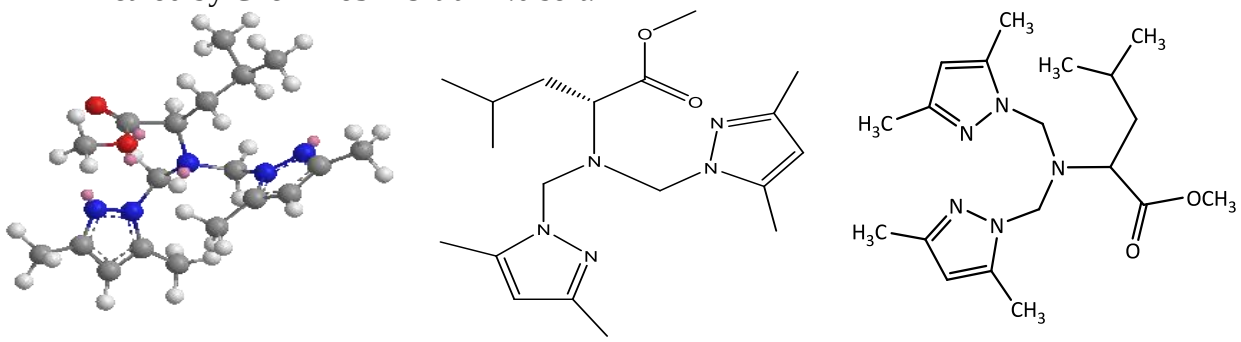

Methyl 2-(bis[(3,5-dimethyl-1*H*-pyrazol-1-yl)methyl]amino)-4-methylpentanoate,**(BT39)**

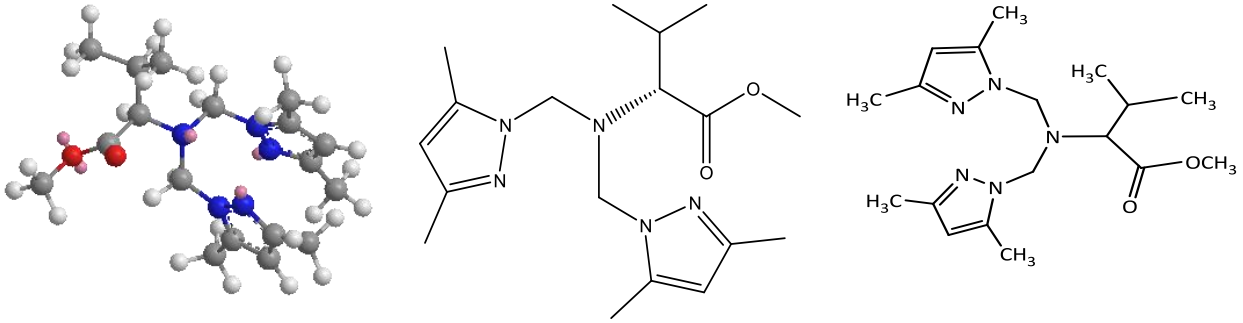

Methyl 2-(bis[(3,5-dimethyl-1*H*-pyrazol-1-yl)methyl]amino)-3-meyhylbutanoate **(BT40)**

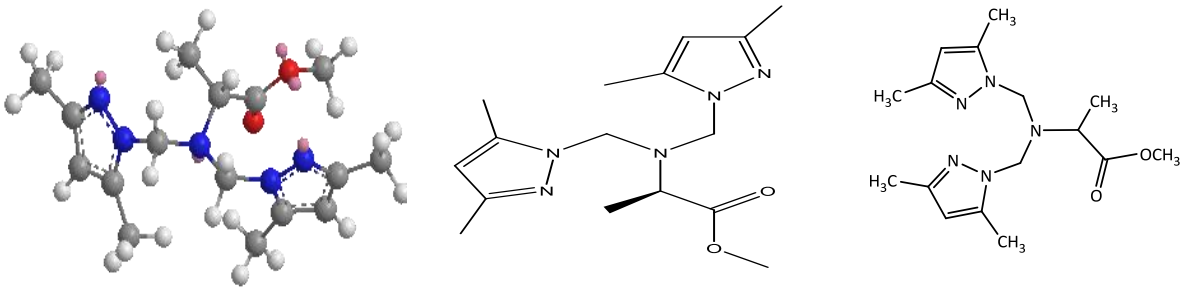

Methyl 2-(bis[(3,5-dimethyl-1H-pyrazol-1-yl)methyl]amino)propanoate **BT (45)**

Figure 1. Name and chemical structures of the investigated organic compounds.

Table 1. Parameters of optimized molecular structures of the studied inhibitors

inhibitors	BT39	BT40	BT 45
Stretch:	2.0563	*2.2106*	1.7025
Bend:	31.0885	*28.3776*	28.4744
Stretch-Bend	0.5220	*0.4471*	0.3335
Torsion	2.5518	*-0.6251*	-0.5756
Non-1,4 VDW	10.6428	*-9.3040*	-8.0944
1,4 VDW:	12.9663	*11.9777*	10.9505
Dipole/Dipole	4.0092	*5.6331*	3.3651
Total Energy	42.5513 kcal/mol	*38.7170 kcal/mol*	36.1562 kcal/mol

2.2. Materials and methods

2.2.1. Gravimetric and polarisation measurement

Prior to all measurements, the steel are polished with different emery paper up to 1200 grade, washed thoroughly with bidistilled water degreased and dried with acetone. The chemical composition of C38 steel is given in Table.2. In order to investigate the effects of temperature and immersion time on the inhibitor performance, some test were carried out in a temperature range 308–353 K.

Table 2. The chemical composition of C38 steel

%C	**%Si**	**%Mn**	**%S**	**%P**	**%Cu**	**%Ni**	**%Cr**	**%N**	**%O**	**%Fe**
0.012	0.01	0.07	0.006	0.008	0.025	0.020	0.015	0.042	0.072	Balance

The aggressive solution (1M HCl) is prepared by dilution of Analytical Grade 37% HCl with double distilled water. Gravimetric measurements are carried out in a double walled glass cell equipped with a thermostated cooling condenser. The solution volume is 100 cm3. The steel specimens used have a rectangular form (2cmx2cmx0.05cm). These sheets are abraded successively with fine

emery paper. The sheets are then rinsed with distilled water, degreased and dried before being weighed and immersed in the corrosive medium. The immersion time for the weight loss is 6 hours at 308K.

The electrochemical study was carried out using a potentiostat PGZ100 piloted by Volta master software. This potentiostat is connected to a cell with three electrode thermostats with double wall (Tacussel Standard CEC/TH). A saturated calomel electrode (SCE) and platinum electrode were used as reference and auxiliary electrodes, respectively. The material used for constructing the working electrode was the same used for gravimetric measurements. The surface area exposed to the electrolyte is 1 cm^2. The data in Tafel region have been processed for evaluation corrosion kinetic parameters by plotting the polarization curves. The linear Tafel segments, in a large domain of potential, of the cathodic curves were extrapolated to the corresponding corrosion potentials to obtain the corrosion current values. The inhibition efficiency was evaluated using the relationship (1). Where, i_{corr}^{0} and i_{corr} are the corrosion current densities values without and with inhibitors, respectively.

$$IE_{I-E} = \frac{i_{corr}^{0} - i_{corr}}{i_{corr}^{0}} \times 100 \qquad (1)$$

The values of the degree of surface coverage (θ) have been obtained from polarization curves for various concentrations of inhibitors. Here, θ can be given as equation .2.

$$\theta = 1 - \frac{i_{corr}}{i_{corr}^{0}} \qquad (2)$$

Potentiodynamic polarization curves were plotted at a polarization scan rate of 0.5mV/s. Before all experiments, the potential was stabilized at free potential during 30 min. The polarisation curves are obtained from −800mV to −200 mV at 308 K. The solution test is there after de-aerated by bubbling nitrogen. Gas bubbling is maintained prior and through the experiments.

The electrochemical impedance spectroscopy (EIS) measurements are carried out with the electrochemical system (Tacussel), which included a digital potentiostat model Voltalab PGZ100 computer at E_{corr} after immersion in solution without bubbling. After the determination of steady-state current at a corrosion potential, sine wave voltage (10 mV) peak to peak, at frequencies between 100 kHz and 10 mHz are superimposed on the rest potential. Computer programs automatically controlled the measurements performed at rest potentials after 30 min of exposure at 308 K. The impedance diagrams are given in the Nyquist representation. Experiments are repeated three times to ensure the reproducibility.

The impedance diagrams were given in the Nyquist representation. To determine the impedance parameters of the C38 steel specimens in acidic solution, the measured impedance data were analyzed using Zview program based upon an electric equivalent circuit [19, 20]. The charge-transfer resistance (Rt) values are calculated from the difference in impedance at lower and higher frequencies. The charge transfer-resistances (R_t) values were calculated from the difference in impedance at low and high frequencies [7, 21-24]. The double layer capacitance (C_{dl}) was obtained at

the frequency fm at which the imaginary component of the impedance is maximal ($Z_{i,\ max}$) by the equation.3.

$$C_{dl} = \frac{1}{2\pi f_m . R_t} \qquad (3)$$

The inhibition efficiency of the inhibitors has been determined from the relationship.4. Where, R_t^0 and R_t are the charge transfer resistance values in the absence and in the presence of inhibitors, respectively.

$$IE_{imp}\% = \frac{R_t - R_t^0}{R_t} \times 100 \qquad (4)$$

2.2.2. Computational Chemistry

DFT method of three-parameter compound functional of Becke and Lyp (B3LYP) was used to study these compounds. The 6-31G* basis set was used for all calculations [25]. To obtain the final stable conformation, calculations of these geometries were performed without constraint on the dihedral angles. The calculations were carried out using the GAUSSIAN 03 program. The theoretical band gaps calculated for isolated chains are expected to be about 0.2 eV larger than condensed phase values. When taking into consideration this difference, we have demonstrated that the B3LYP/6-31G(d) method has the particularity to reproduce gap [26, 27] values similar to those of the experience. The following quantum chemical indices are considered: the energy of the highest occupied molecular orbital (E_{HOMO}), the energy of the lowest unoccupied molecular orbital (E_{LUMO}), $\Delta E = E_{HOMO} - E_{LUMO}$, total charge density calculated by extended Huckel and the dipole moment (μ) [28-30].

3. RESULTS AND DISCUSSION

3.1. Weight loss methods.

Weight loss of C38-steel, in mg cm^{-2} of the surface area, was determined at different concentration in the absence and presence of the new synthetised methyl2-(bis[(3,5-dimethyl-1*H*-pyrazol-1-yl)methyl]amino)-4-methylpentanoate (BT39), Methyl2-(bis[(3,5-dimethyl-1*H*-pyrazol-1 yl)methyl]amino)-3-meyhylbutanoate (BT40) and methyl 2-(bis[(3,5-dimethyl-1H-pyrazol-1-yl)methyl]amino)propanoate (BT45) at 298K. From the weight loss results, the corrosion rate (CR), the inhibition efficiency (η_{WL}(%)) of the inhibitor and degree of surface coverage (θ) were calculated using equations 5, 6 and 7 [7, 23];

$$C_R = \frac{W_b - W_a}{At} \qquad (5)$$

$$\eta_{WL}(\%) = \left(1 - \frac{w_i}{w_0}\right) \times 100 \quad (6)$$

$$\theta = 1 - \frac{w_i}{w_0} \quad (7)$$

where W_b and W_a are the specimen weight before and after immersion in the tested solution, w_0 and w_i are the values of corrosion weight losses of carbon steel in uninhibited and inhibited solutions, respectively, A the total area of the carbon steel specimen (cm^2) and t is the exposure time (h) and θ is the degree of surface coverage of the inhibitor..

The values of $\eta_{WL}(\%)$ for all inhibitors are given in Table 3.This show that the inhibition efficiency increases with the increasing inhibitor concentration. These results reveal that the compounds under investigation are fairly efficient inhibitors for C38-steel dissolution in 1.0 M HCl solution. The inhibition of corrosion of C38-steel by bipyrazol derivatives can be explained in terms of adsorption on the metal surface. These compounds can be adsorbed on the C38-steel surface by the interaction between lone pairs of electrons of nitrogen atoms of the inhibitors and the metal surface. This process is facilitated by the presence of vacant orbital of low energy in iron atom, as observed in the transition group elements. Careful inspection of these results showed that, the ranking of the inhibitors according to $\eta_{WL}(\%)$ is as follows: BT(45) > BT(40) > BT(39) for the same concentration.

Table 3. Corrosion parameters obtained from weight loss measurements for carbon steel in 1.0 M HCl containing various concentrations of inhibitors at 308 K.

Inhibitors	Conc (M)	$10^{-4}\times CR$ (mg cm^{-2} h^{-1})	$\eta_{WL}(\%)$	Θ
Blank	1	0.77	-	-
(BT39)	10^{-6}	0.639	17	0.17
	10^{-5}	0.471	38	0.38
	$5x10^{-5}$	0.449	41	0.41
	10^{-4}	0.411	46	0.46
	$5x10^{-4}$	0.358	53	0.53
	10^{-3}	0.340	56	0.56
(BT40)	10^{-6}	0.542	29	0.29
	10^{-5}	0.482	37	0.37
	$5x10^{-5}$	0.435	43	0.43
	10^{-4}	0.335	56	0.56
	$5x10^{-4}$	0.329	57	0.57
	10^{-3}	0.289	62	062
(BT45)	10^{-6}	0.696	10	0.10
	10^{-5}	0.477	38	0.38
	$5x10^{-5}$	0.304	60	0.60
	10^{-4}	0.300	61	0.61
	$5x10^{-4}$	0.190	75	0.75
	10^{-3}	0.091	88	0.88

Compared with (BT45), (BT40) and (BT39), the higher inhibition effect of (BT45) may be attributed to the group propanoate in the position by a group meyhylbutanoate and methylpentanoate respectively for (BT40) and (BT39). In this way, a correlation between the electronic parameters (induction and mesomeric effects of the substituent and steric effect) as well as chemical structure (molecular area) and inhibition property is effective [42]. Also, the larger molecular size of (BT45) can be considered which ensures greater coverage of the metallic surface [5, 6, 31, 32].

The variation of corrosion rate and efficiencies with concentration of inhibitor has been found off these compounds inhibits the corrosion of C38-steel in HCl solution at all concentrations used in this study. It has also been observed that the inhibition efficiency for these compounds increases with the increase in concentration. Maximum η_{WL}(%) for these compounds was achieved at 10^{-3}M and attained 88% for (BT45).

3.2. Effect of temperature.

Temperature can affect the steel corrosion in the acidic media in the presence and absence of inhibitor. Generally the corrosion rate increases with the rise of the temperature. Temperature can affect the steel corrosion in the acidic media in the presence and absence of inhibitor. To determine the action energy of the corrosion process, gravimetric measurements are taken at various temperatures (313–353K) in the presence and absence of 10^{-3}M of (BT45) at 1 hour of immersion. The corresponding results are given in Table 4.

Table 4. Effect of temperature on the corrosion of steel with and without 10^{-3}M of (BT45).

Temperature (K)	Blank	**(BT45)**	
	W^0_{corr} (mg/ cm^2.h)	**W_{corr} (mg/ cm^2.h)**	**E(%)**
313	0.7418	00.1335	82
323	1.4576	00.5685	61
333	2.8921	01.2436	57
343	11.330	05.0985	55
353	31.301	17.2155	45

It is clear that the increase of corrosion rate is more pronounced with the rise of temperature for the blank solution. In the presence of the tested molecules, W_{corr} is reduced even at high temperature. *E* (%) passed from 82 to 45% when temperature rises from 313 to 353 K at 10^{-3} M of **(**BT45). We note that the efficiency of the inhibitors tested depends on the temperature and decreases with the rise of temperature from 313 to 353 K.

The apparent activation for the corrosion process is calculated from Arrhenius type plot according to the following equation 8. [16, 33, 34]:

$$W = k \exp\left(-\frac{E_a}{RT}\right) \qquad (8)$$

where E_a is the apparent activation corrosion energy, R is the universal gas constant, k is the Arrhenius pre-exponential constant and T is the absolute temperature. Arrhenius plots for the corrosion rate of mild steel are given in Figure. 2. Values of E_a for mild steel in 1 M HCl with the absence and presence various concentrations of (BT45) were determined from the slope of ln (W) vs. 1/T plots and shown in Table 4. The value of apparent activation energy E_a of hydrogen evolution reaction for 1 M HCl $_{without}$ an inhibitor (37.87 kJ mol^{-1}) agrees well with literature data on E_a for steel in norm al hydrochloric acid [20-22]. In the presence of (BT45) inhibitor, the process of metal dissolution is characterized by activation energy less than that in the uninhibited 1 M HCl (Table 4). The addition of inhibitor modified the values of E_a (47.50 kJ mol^{-1}); this modification may be attributed to the change in the mechanism of the corrosion process in the presence of adsorbed inhibitor molecules [3, 35-40]. The lower value of the activation energy of the process in an inhibitor's presence when compared to that in its absence is attributed to its chemisorptions, while the opposite is the case with physical adsorption [41-45] .

The lower value of the E_a was attributed both a slow rate of inhibitor adsorption with a resultant closer approach to equilibrium during the experiments at the higher temperature. The decrease in activation energy of corrosion at higher levels of inhibition arises from a shift of the net corrosion reaction from that on the uncovered part on the metal surface to the covered one. The organic molecules inhibit both the anodic and cathodic partial reactions on the electrode surface and a parallel reaction takes place on the covered area, but that the reaction rate on the covered area is substantially less than on the uncovered area. An alternative formulation of Arrhenius equation is [31]:

$$W = \frac{RT}{Nh} \exp\left(\frac{\Delta S_a^o}{R}\right) \exp\left(-\frac{\Delta H_a^o}{RT}\right) \qquad (6)$$

where h is plank's constant, N is Avogadro's number, ΔS_a^0 is the entropy of activation and ΔH_a^0 is the enthalpy of activation. Figure. 2 show a plot of ln (W/T) against 1/T in the absence and presence of the inhibitors. A straight lines are obtained with a slope of ($-\Delta H_a^0/R$) and an intercept of (Ln R/Nh + $\Delta S_a^0/R$) from which the values of ΔH_a^0 and ΔS_a^0 are calculated, are listed in Table 5. The relationship between the activation energy E_a and activation heat ΔH_a^0 against the concentration of all inhibitors is shown in Figure. 3. From the data obtained in Table 5, it seems that E_a and ΔH_a^0 vary in the same manner; these results agree those obtained in the literature [5, 6, 31, 46]. The positive signs of the enthalpies (ΔH_a^0) reflect the endothermic nature of the steel dissolution process (Table 5). Large and negative values of entropies (ΔS_a^0) imply that the activated complex in the rate determining step represents an association rather than a dissociation step, meaning that a decrease in disordering takes place on going from reactants to the activated complex.

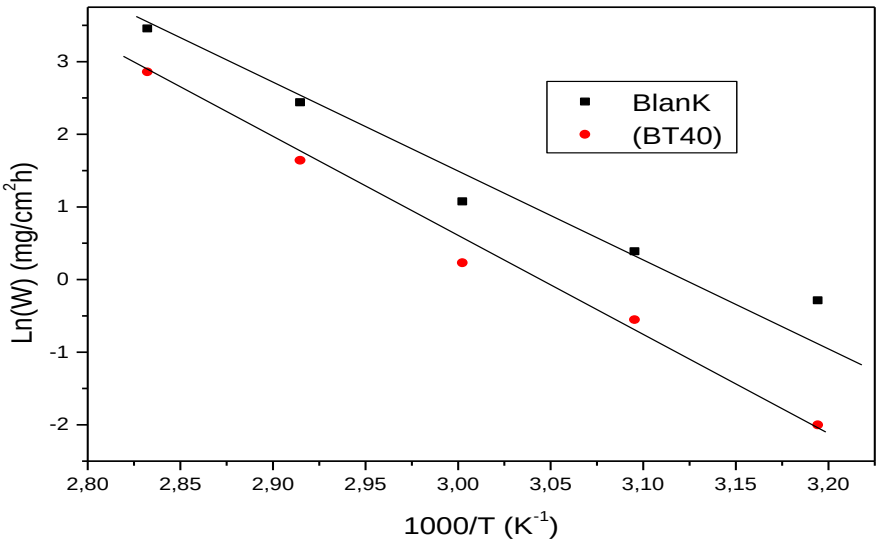

Figure 2. Arrhenius plots for steel in 1M HCl in the absence and presence of (BT45).

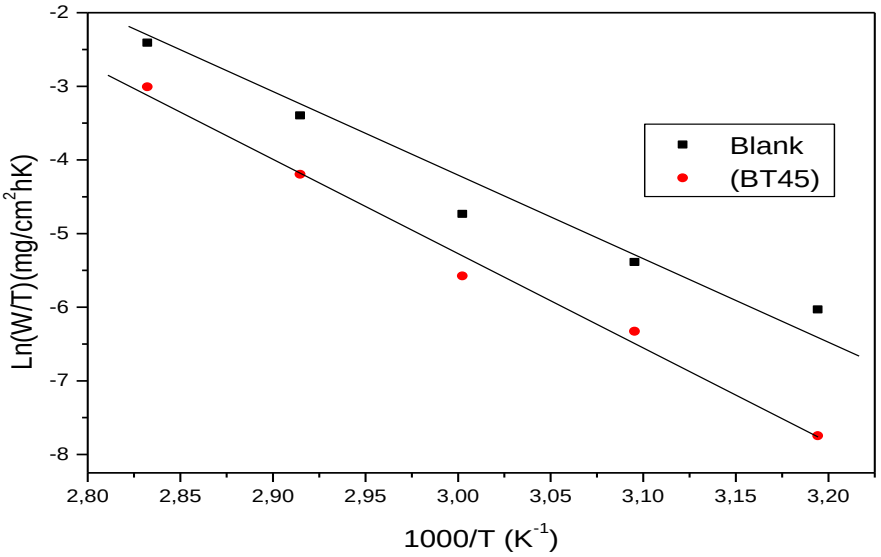

Figure 3. Ln (w/T) as function of 1/I for steel in 1M HCl in the absence and presence of (BT45).

Table 5. thermodynamic parameters at different concentrations

inhibitors	Linear coefficient regression (r)	E_a (kJ/mol)	$\Delta H_a°$ (kJ/mol)	$\Delta Sa°$ (kJ/mol)
HCl	0.9850	37.87	36.67	19.65
BT45	0.9899	47.50	46.30	59.10

3.3. Tafel extrapolation

Polarization measurements have been carried out in order to gain knowledge concerning the kinetics of the anodic and cathodic reactions. Potentiodynamic curves are obtained in the presence and absence of the studied inhibitors, after pre-polarizing the electrode at its E_{corr} for one hour, thereafter pre-polarized at -800 mV for 10 min. After this scan, the potential was swept stepwise from the most cathodic potential to the anodic direction.

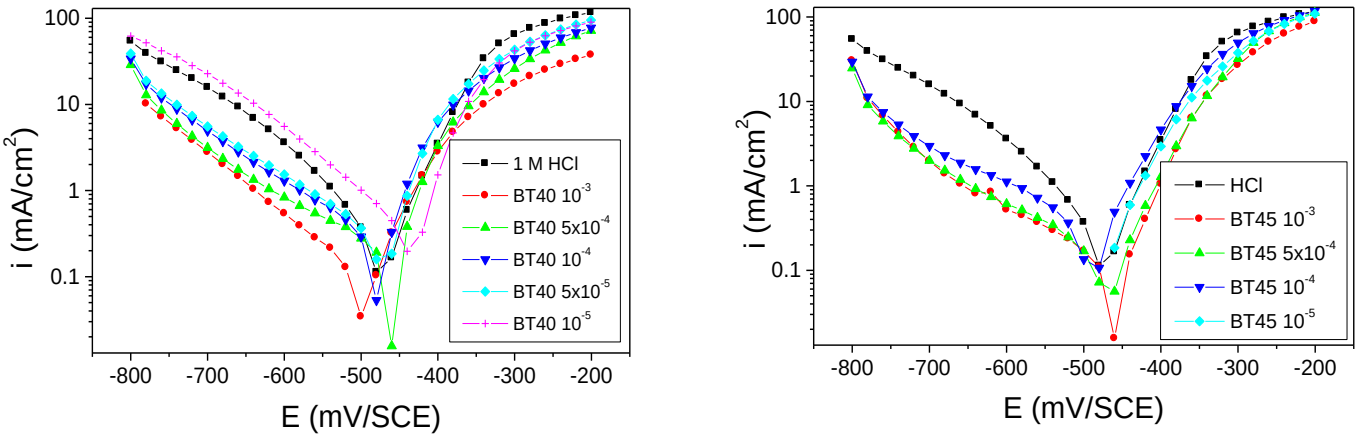

Figure 4. Polarisation curves of steel in 1M HCl at different concentrations of (BT40) and (BT45)

The effect of rise concentration of (*BT39),* (*BT40)* and (*BT45)* on the anodic and cathodic polarisation curves of mild steel in 1 M HCl at 298 K is presented in Figure. 4. Various corrosion parameters such as corrosion current densities (i_{corr}), corrosion potentials (E_{corr}), cathodic Tafel slopes (βc), degree of surfaces coverage (θ) and inhibition efficiencies $IE_{I\text{-}E}$%, obtained from polarization measurements are listed in Table 6.

From the recorded results, we can conclude that in all cases, addition of the studied compounds induced a marked decrease in the cathodic and a slight decrease in the anodic current densities. Accordingly, these inhibitors affect greatly the hydrogen reaction discharge and slightly affect the mild steel dissolution processes. The hydrogen evolution reaction is under activation control since the cathodic portions rise to Tafel lines. The fact that cathodic process slow down can be due to the covering of the surface with monolayer of the tested molecules due to the adsorbed inhibitors on the mild steel surface then reducing the electrolyte infiltration to the interface. This idea is investigated in separate section by plotting of suitable adsorption isotherm.

The results obtained by this electrochemical method are very similar to those obtained by the gravimetric method. The agreement between the two methods is very satisfactory. The order of inhibition efficiency of the tested compounds decreases in the following sense.

(BT45) >(BT40) > (BT39)

Table 6. Values of electrochemical parameters evaluated from the cathodic current-voltage characteristics for the system electrode/1 M HCl with and without added inhibitors at 298 K

Inhibitor	*Concentration mol L^{-1}*	*E_{corr} mV$_{sce}$*	*$\mid \beta_c \mid$ mV dec^{-1}*	*i_{corr} μA cm^{-2}*	*IE_{I-E} %*
Blank	1	-472	-147	494.8	-
(BT39)	10^{-6}	-446	-184	425.5	14
	10^{-5}	-444	-101	395.8	20
	$5x10^{-5}$	-454	-182	311.7	37
	10^{-4}	-463	-172	277.1	44
	$5x10^{-4}$	-453	-215	247.4	50
	10^{-3}	-429	-153	223.1	55
(BT40)	10^{-6}	-469	-167	390.0	21
	10^{-5}	-431	-138	366.1	26
	$5x10^{-5}$	-469	-175	264.6	46
	10^{-4}	-476	-165	214.4	57
	$5x10^{-4}$	-462	-175	187.3	62
	10^{-3}	-494	-141	108.3	78
(BT45)	10^{-6}	-475	-159	405.9	18
	10^{-5}	-474	-205	262.2	29
	$5x10^{-5}$	-463	-167	163.7	47
	10^{-4}	-489	-179	194.5	60
	$5x10^{-4}$	-468	-166	80.4	83
	10^{-3}	-459	-169	67.8	86

3.4. Electrochemical impedance spectroscopy measurements

The corrosion behaviour of steel, in acidic solution in the presence of (BT45), (BT40) and (BT39) at different concentrations was investigated by EIS measurements at room temperature. As observed, the Nyquist plots contain a depressed semi-circle with the centre below the real X-axis, which is size increased by increasing the inhibitor concentrations, indicating that the corrosion is mainly a charge transfer process [47-49] and the formed inhibitive film was strengthened by the addition of (BT45), (BT40) and (BT39) compounds . The depressed semi-circle is the characteristic of solid electrodes and often refers to the frequency dispersion which arises due to the roughness and other in homogeneities of the surface. It is worth noting that the change in concentration of (BT45), (BT40) and (BT39) did not alter the style of the impedance curves, suggesting a similar mechanism of the inhibition is involved.

The equivalent circuit model employed for this system is as previously reported by fitting with Zview program [50] is showed in the in Figure.5. Nyquist plots of steel in inhibited and uninhibited acidic solutions containing various concentrations of sulphuric compounds are shown in Figure.5. The charge-transfer resistance (R_t) values are calculated from the difference in impedance at lower and higher frequencies. To obtain the double layer capacitance (C_{dl}) the frequency at which the imaginary component of the impedance is maximal ($-Z_{max}$) is found as represented in equation.9. [3, 51-53] .

$$C_{dl} = \frac{1}{\omega.R_t} \quad \text{Where} \quad \omega = 2\pi f_{max} \qquad (9)$$

The inhibition efficiency obtained from the charge transfer resistance is calculated by equation.10.:

$$E(\%) = \frac{\left[R_{t/inh} - R_t\right]}{R_{t/inh}}.100 \qquad (10)$$

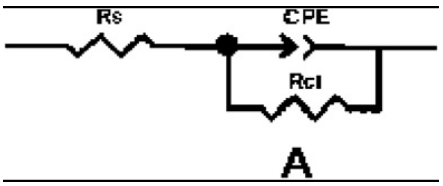

Figure 6. Equivalent circuit used in the modelling of the EIS data

R_t and $R_{t/inh}$ are the charge transfer-resistance values with and without inhibitor, respectively. The charge transfer resistance, R_t, the double layer capacitance C_{dl}, the frequency f_{max} values were given in Table.7.

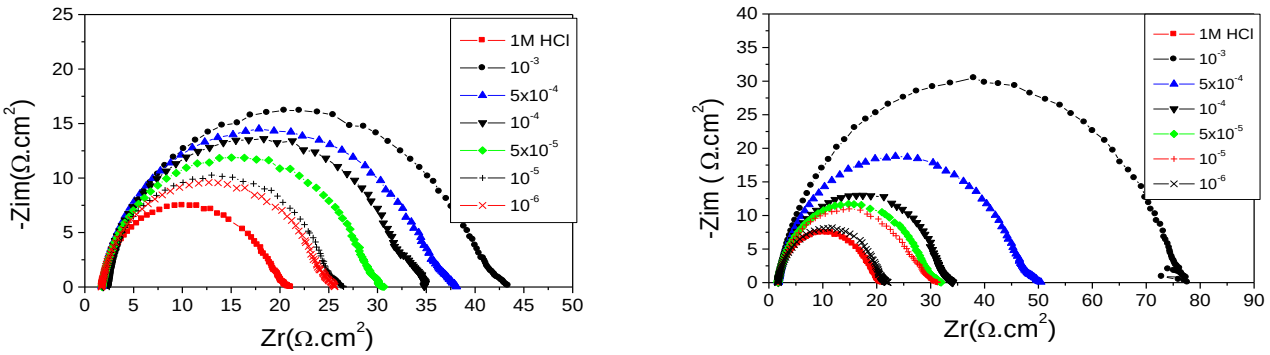

Figure 5. Nyquist diagrams for steel in 1M HCl with different concentrations of (BT39) and (BT45).

The obtaining of the semicircle in the impedance diagrams indicated that the corrosion of steel is controlled by a charge transfer process. Table 7 shows the impedance parameters obtained by line fitting to the semicircle. The charge transfer resistance (R_t) increases with the inhibitor concentration. Also, the double layer capacitance (C_{dl}) decreases with increase in the concentration of the inhibitor. This decrease is due to the adsorption of the inhibitor at the metal surface causing a change of the double layer structure [54-57]. When comparing the inhibition efficiencies obtained from testing

methods used in this study, it can be concluded that there is a fair agreement between results obtained by different techniques used

Table 7. The impedance data for steel in 1M HCl for various concentrations of all inhibitors

Inhibitors	concentration	R_t / Ω cm^2	F_{max} / Hz	C_{dl} / μF cm^{-2}	E / %
Blanc	1 M	15.414	12.50	74.23	-
(BT39)	10^{-6}	18.351	11.11	63.52	16
	10^{-5}	21.323	08.93	56.99	28
	$5x10^{-5}$	25.412	07.93	53.67	39
	10^{-4}	29.018	06.33	46.02	47
	$5x10^{-4}$	31.849	07.14	46.30	52
(BT40)	10^{-6}	19.021	11.16	62.25	19
	10^{-5}	20.751	10.00	57.47	26
	$5x10^{-5}$	24.469	10.90	48.74	37
	10^{-4}	28.544	11.00	38.28	46
	$5x10^{-4}$	37.595	08.92	38.00	59
(BT45)	10^{-6}	20.281	10.00	65.69	24
	10^{-5}	23.767	05.00	51.20	35
	$5x10^{-5}$	25.585	05.62	51.00	43
	10^{-4}	45.335	07.14	43.34	66
	$5x10^{-4}$	59.952	07.14	39.87	74
	10^{-3}	71.581	05.89	33.42	78

3.5. Adsorption isotherm

Basic information on the interaction between the inhibitors and the steel surface is provided by the adsorption isotherm. In order to evaluate this isotherm, the degree of surface coverage θ for different concentrations of the inhibition in acidic media of different compounds has been evaluated from weight loss using the equation.11. [6, 58]:

$$\theta = \frac{W_{(\theta=0)} - W_{\theta}}{W_{(\theta=0)} - W_{(\theta=1)}} \qquad (11)$$

The surface coverage values θ were tested graphically for fitting a suitable adsorption isotherm. The plot of C_{inh}/θ versus C_{inh} yields a straight line, proving that the adsorption of the inhibitors from HCl solution on the steel surface obeys the Langmuir adsorption isotherm (Figure. 6) which obeys to equation.12 and 13:

$$\frac{C_{inh}}{\Theta} = \frac{1}{b} + C_{inh} \qquad (12)$$

$$b = \frac{1}{55,5}.\exp(-\frac{\Delta G°_{ads}}{R.T}) \quad (13)$$

C_{inh} is the inhibitor concentration; θ is the fraction of the surface covered, b is the adsorption coefficient and $\Delta G°_{ads}$ is the standard free energy of adsorption.

The obtained plot of inhibitors is linear. The intercept permit the calculation of the equilibrium constant b which leads to evaluate ΔG°_{ads}((BT39)) = -36.22 kJ/mol, ΔG°_{ads}((BT40)) = -41.13 kJ/mol, ΔG°_{ads}((BT45)) = - 35.48 kJ/mol. The results show that the all inhibitors gives negative of $\Delta G°_{ads}$ indicating that it is strongly adsorbed on the metal surface. In general, the negative values of $\Delta G°_{ads}$ indicate the spontaneous adsorption of inhibitors on the steel surface [4, 59, 60]. This value indicates that inhibitor interacts on the steel surface by electrostatic effect.

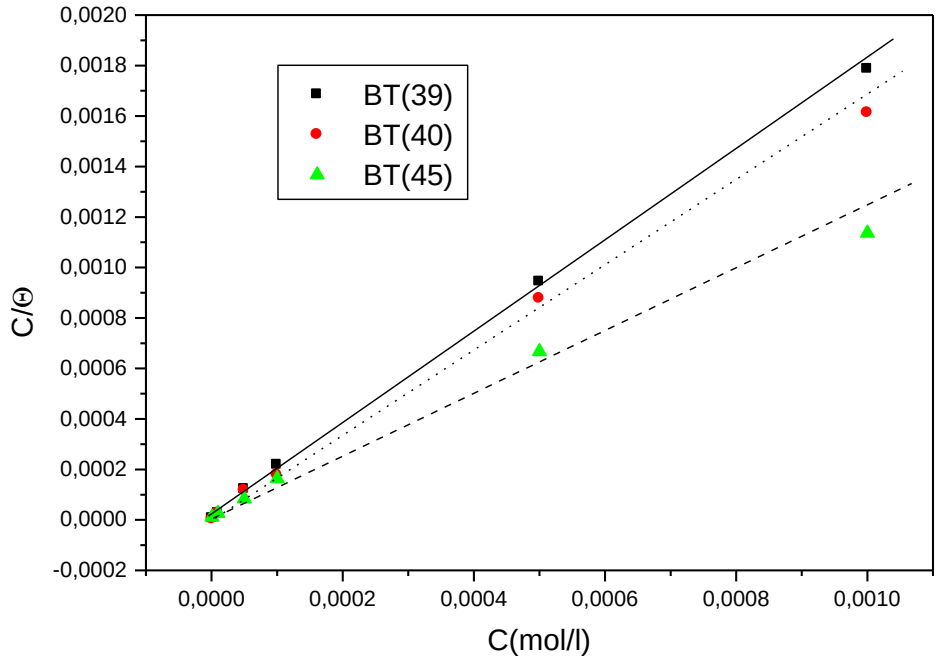

Figure 6. Langmuir isotherm adsorption model of inhibitors on the surface of steel in 1M HCl

3.6. Relationships between inhibition efficiency and global quantum chemical data

Bipirazolic derivatives as corrosion inhibitors are investigated experimentally. (BT39), (BT40) and (BT45) differ by substituent and have inhibiting effectiveness varying than the effectiveness of (BT45) is higher. Quantum chemical calculations are developed to get more information on the molecular state more stable and performed to investigate the structural parameters affect the inhibition efficiency of inhibitors and study their adsorption mechanisms on the metal surface.

Quantum chemical calculations permit also to get geometric and electronic structures of the inhibitors by optimizing of their bond lengths, bond angles and dihedral angles. Figure. 2 present the optimized molecular structures of the studied inhibitors. The calculations which are responsible for the inhibition efficiency of inhibitors such as the energies of highest occupied molecular orbital (E_{HOMO}),

energy of lowest unoccupied molecular orbital (E_{LUMO}), the separation energy (E_{LUMO} - E_{HOMO}), ΔE, representing the function of reactivity, the net charge on the functional group and dipole moment, μ, are collected in Table 8 [14, 28, 29, 61, 62].

Table 9: Mulliken charge of different inhibitors.

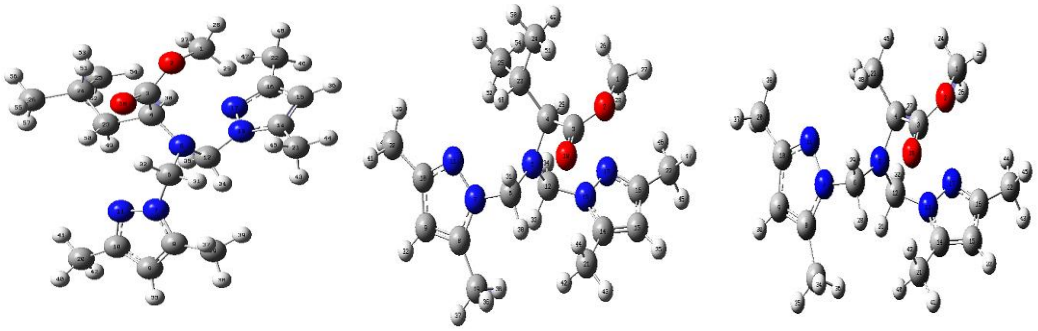

Number	Atom	Mulliken Charge of (BT39)	Mulliken Charge of (BT40)	Mulliken Charge of (BT45)
1	C	-0,107	-0,111	0,289
2	O	-0,452	-0,454	-0,448
3	C	0,619	0,627	0,632
4	C	-0,036	-0,026	0,080
5	N	-0,444	-0,397	-0,382
6	C	0,085	0,079	0,338
7	N	-0,338	-0,322	-0,322
8	C	0,347	0,355	0,356
9	C	-0,252	-0,255	-0,183
10	C	0,306	0,306	0,307
11	N	-0,353	-0,354	-0,357
12	C	0,098	0,077	0,340
13	N	-0,312	-0,333	-0,332
14	C	0,347	0,358	0,366
15	C	-0,247	-0,239	-0,162
16	C	0,286	0,290	0,296
17	N	-0,356	-0,364	-0,368
18	O	-0,465	-0,479	-0,474
19	C	-0,384	-0,388	-0,007
20	C	-0,376	-0,376	-0,018
21	C	-0,392	-0,394	0,006
22	C	-0,377	-0,378	-0,017
23	C	-0,144	-0,049	0,062
24	C	-0,071	-0,339	
25	C	-0,319		
26	C	-0,310		

The effectiveness of an inhibitor can be related to its spatial molecular structure, as well as with their molecular electronic structure. Also there are certain quantum chemical parameters that can be related to the interactions metal-inhibitor. Among these, we can mention the energy of the HOMO, which is often associated with the capacity of a molecule to donate electrons. Therefore, an increase in the values of E_{HOMO} can facilitate the adsorption and therefore the inhibition efficiency, by

indicating the disposition of the molecule to donate orbital electrons to an appropriate acceptor with empty molecular orbitals. In the same way low values of the energy gap $\Delta E = E_{LUMO} - E_{HOMO}$ will render good inhibition efficiencies, because the energy needed to remove an electron from the last occupied orbital will be low [28, 62]. Similarly, low values of the dipole moment l will favour the accumulation of inhibitor molecules on the metallic surface. The optimized geometry of (BT39), (BT40) and (BT45) is shown in Figure. 7. The Mulliken charge densities of (BT39), (BT40) and (BT45), have the following values Table 8, have been calculated [26, 63, 64]. The results seem to indicate that both the value of the gap energy ΔE, as well as the value obtained for the dipole moment, favour the (BT45), implying its effectiveness as a corrosion inhibitor. A similar result was obtained.

The use of Mulliken population analyses to probe the adsorption centres of inhibitors has been widely reported. The level of theory (DFT) used in this work has been reported by us and others and was shown to give good results [14, 25]. There is a general consensus by several authors that the more negatively charged and heteroatom is the more it can be adsorbed on the metal surface through donor–acceptor type reaction. It has also been reported that electrophiles attack molecules at sites of negative charge, which means that sites of ionic reactivity can be estimated from the atomic charges in a molecule. Thus, from the values of Mulliken charge in Table 8, it is possible to observe that all the nitrogen and oxygen atoms present a considerable excess of negative charge and negative charges around most carbon atoms of the aromatic rings. Accordingly, the (BT39), (BT40) and (BT45) molecules can be adsorbed on the Al surface using these active centres leading to the corrosion inhibition action.

E_{HOMO} is a quantum chemical descriptor which is often associated with the electron donating ability of the molecule. High value of E_{HOMO} is likely to indicate a tendency of the molecule to donate electrons to appropriate acceptor molecule of low empty molecular orbital energy. Therefore, the energy of the lowest unoccupied molecular orbital, E_{LUMO}, indicates the ability of the molecule to accept electrons. So, the lower the value of E_{LUMO}, the more probable the molecule accepts electrons [28]. The binding ability of the inhibitor to the metal surface increases with increasing of the HOMO and decreasing of the LUMO energy values.

The calculations show that the (BT39), (BT40) and (BT45) are the highest HOMO level respectively at –0.2210, -0.2212 and -0.2190 a. u. The lowest LUMO level at 0.0096, 0.0050 and 0.0047 a. u. This can explain that the highest inhibition efficiency of (BT39), (BT40) and (BT45) molecule are due to the increasing energy of the HOMO and the decreasing energy of the LUMO. This is in a good agreement with the experimental observations suggesting that the (BT39), (BT40) and (BT45) are the highest inhibition efficiency among the investigated inhibitors. The separation energy, $\Delta E = (E_{LUMO} - E_{HOMO})$, is an important parameter as a function of reactivity of the inhibitor molecule towards the adsorption on metallic surface. As ΔE decreases, the reactivity of the molecule increases leading to increase the inhibition efficiency of the molecule

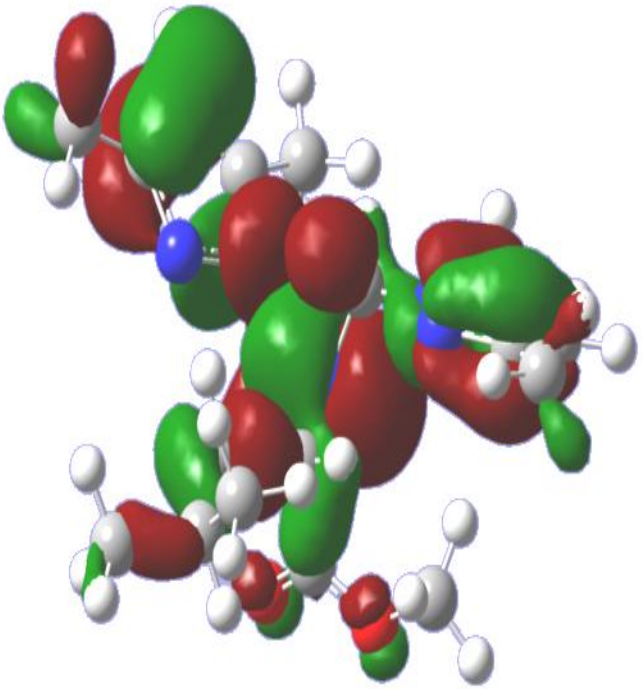

HOMO for (BT39)

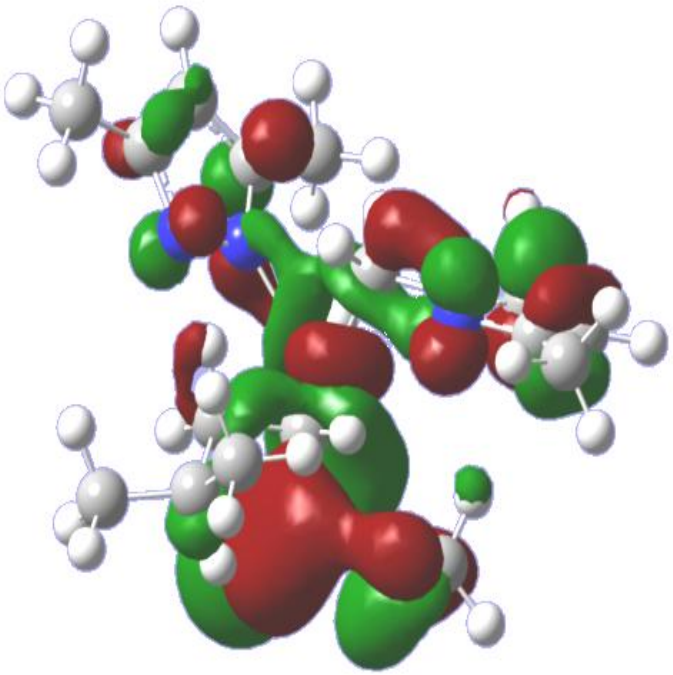

LUMO for (BT39)

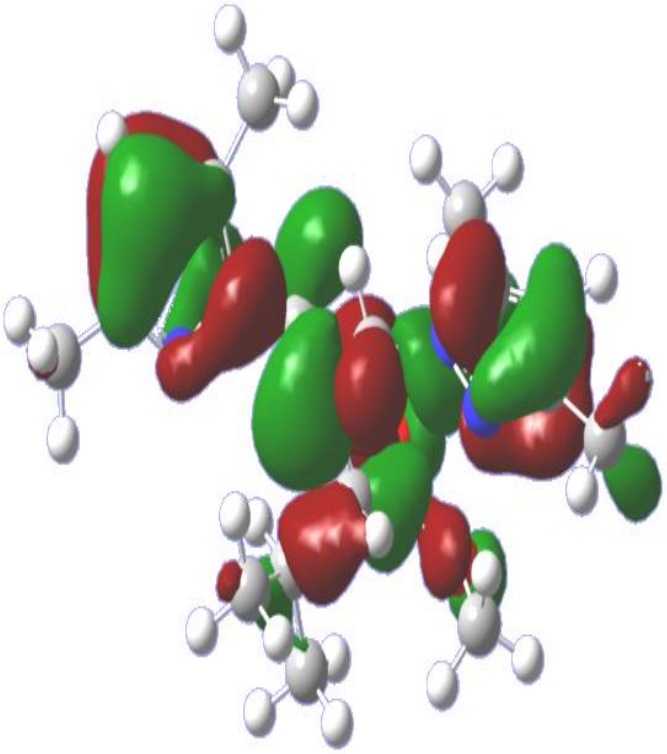

HOMO for (BT40)

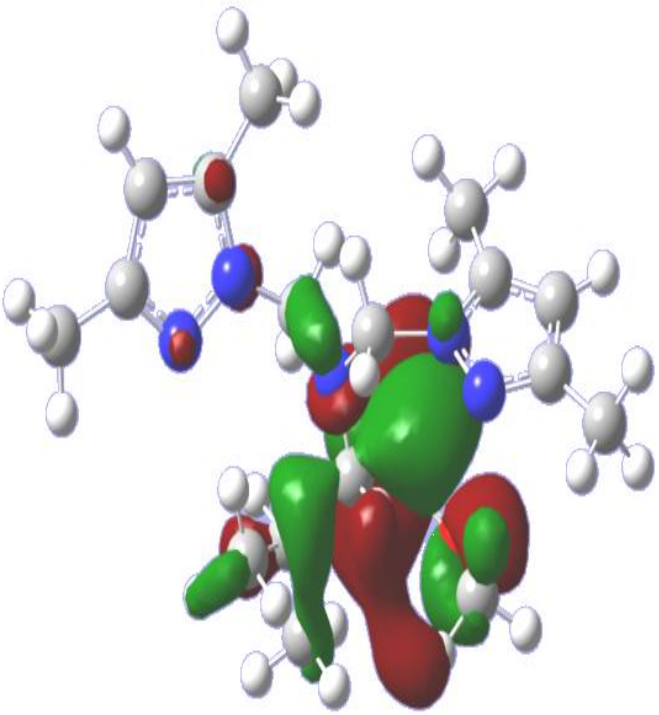

LUMO for (BT40)

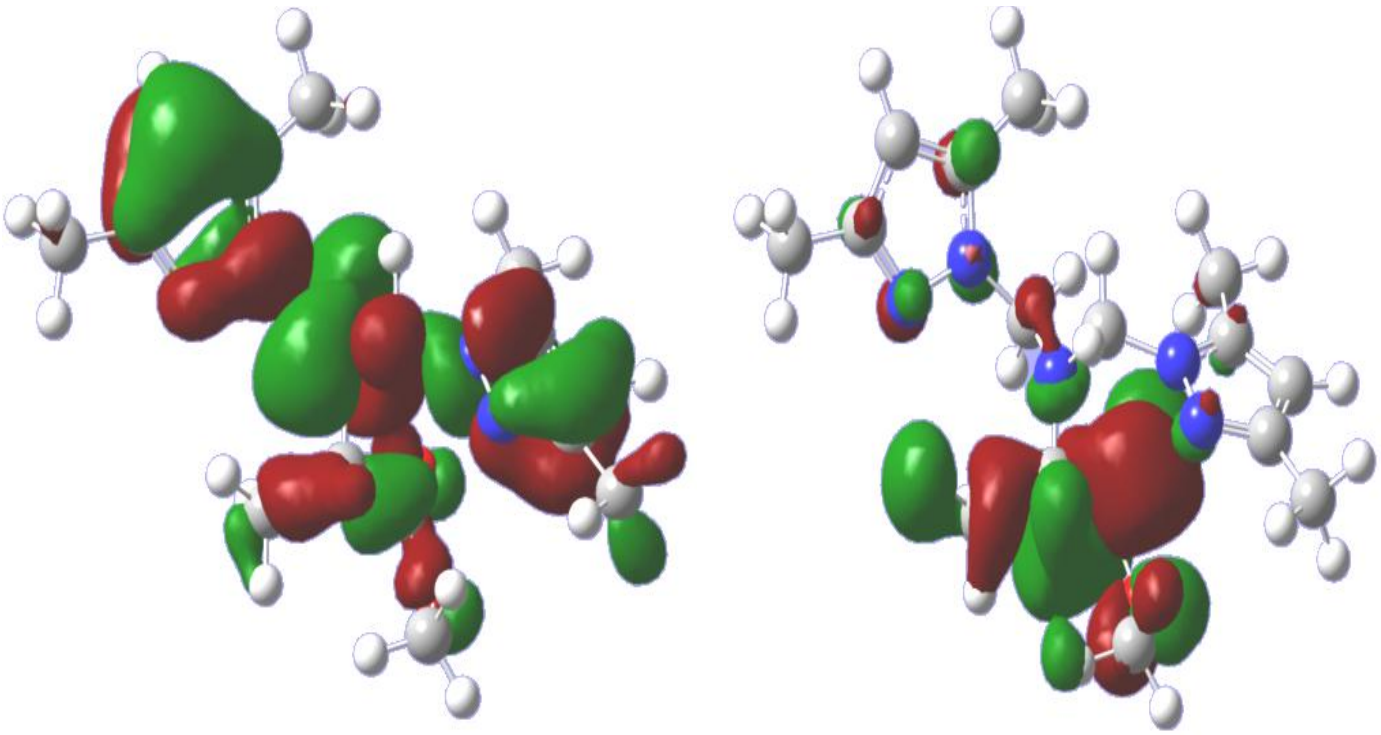

HOMO for (BT45) LUMO for (BT45)

Figure 7. the HOMO and LUMO of (BT39), (BT40) and (BT45)

It has been assumed that organic inhibitor molecules establish their inhibition action via the adsorption of the inhibitor onto the metal surface. The adsorption process is affected by the chemical structures of the inhibitors, the nature and charged surface of the metal and the distribution of charge over the whole inhibitor molecule. In general, two modes of adsorption can be considered.

Table 9. the calculated quantum chemical parameters of the bipyrazol derivatives

Inhibitors	HOMO (a. u)	LUMO (a. u)	ΔE (a. u)	μ (Debye)
BT39	-0.2210	0.0096	0.2306	4.5539
BT40	-0.2212	0.0050	0.2260	2.1959
BT45	-0.2190	0.0047	0.2237	1.7414

The physical adsorption requires the presence of electrically charged metal surface and charged species in the bulk of the solution. Chemisorptions process includes charge sharing or charge transfer from the inhibitor molecule to the metal surface. The presence of the transition metal having vacant orbital of low energy with the inhibitor molecule having relatively loosely bound electrons or hetero atom with lone pair of electrons facilitates this adsorption

4. CONCLUSION

- The (BT39), (BT40) and (BT45), substantially inhibit corrosion of steel alloy by acid; BT45 is an especially good inhibitor.
- Cathodic-type inhibition was observed, corrosion is controlled by a charge transfer process, and the process of corrosion is unaffected by the presence of the inhibitors.
- Inhibition is because of adsorption of the inhibitor molecules on the steel surface, thus blocking its active sites. Adsorption of the inhibitors fits a modified Langmuir isotherm model; physical
- Adsorption and chemisorptions both occur.
- Theoretical calculations (quantum chemical) are in good agreement with results obtained from electrochemical study and structure–corrosion protection relationships, which also confirm that the adsorption centre is N atoms.

ACKNOWLEDGEMENTS
Prof S. S. Al-Deyab and Prof B. Hammouti extend their appreciation to the Deanship of Scientific Research at king Saud University for funding the work through the research group project.

References

1. I. Belfilali, A. Chetouani, B. Hammouti, A. Aouniti, S. Louhibi, S.S. Al-Deyab, *Int. J. Electrochem. Sci.*, 7 (2012) 3997.
2. Khaled, K. F., El-mghraby, A., Ibrahim, O. B., Elhabib, O. A., Magdy A. M. Ibrahim, *J. Mater. Environ. Sci*. 1 (2010) 139.
3. A. Chetouani, K. Medjahed, S.S. Al-Deyab, B. Hammouti, I. Warad, A. Mansri, A. Aouniti, *Int. J. Electrochem. Sci.*, 7 (2012) 6025.
4. S. El Ayyoubi, A. Chetouani, Hammouti, A. Warthan, A. Mansri, S.S. Al-Deyab, *Int. J. Electrochem. Sci.* 7 (2012) 1639.
5. M. Benabdellah, B. Hammouti, A. Warthan, S.S. Al-Deyab, C. Jama, M. Lagrenee, F. Bentiss, *Int. J. Electrochem. Sci.*, 7 (2012) 3489.
6. F. Bentiss, M. Outirite, M. Traisnel, H. Vezin, M. Lagrenee, B. Hammouti, S.S. Al-Deyab, C. Jama, *Int. J. Electrochem. Sci.*, 7 (2012) 1699.
7. A. Chetouani, B. Hammouti, T. Benhadda, M. Daoudi, *App. Surf. Sci.*, 249 (2005) 375.
8. M.R. Arshadi, M.G. Hosseini, M. Ghorbani, *Br. Corros. J.*, 37 (2002) 76.
9. R. A. Mohammed, M. Abdulwahab, I. A. Madugu, J. O. Gaminana, F. Asuke, *J. Mater. Environ. Sci*. 4 (2013) 93.
10. O. Benali, H. Benmehdi, O. Hasnaoui, C. Selles, R. Salghi, *J. Mater. Environ. Sci.* 4 (2013) 127.
11. N.O. Eddy, A.O. Odiongenyi, P.O. Ameh, E.E. Ebenso, *Int. J. Electrochem. Sci.* 7 (2012) 7425.
12. N.O. Eddy, F.E. Awe, A.A. Siaka, L. Magaji, E.E. Ebenso, *Int. J. Electrochem. Sci.* 6 (2011) 4316.
13. L. Herrag, M. Bouklah, N.S. Patel, B.M. Mistry, B. Hammouti, S. Elkadiri, M. Bouachrine, *Res. Chem. Intermed.*, 38 (2012) 1669.
14. M. Bouklah, H. Harek, R. Touzani, B. Hammouti, Y. Harek, *Arab. J. Chem.*, 5 (2012) 163.
15. S.M.A. Hosseini, M. Salari, E. Jamalizadeh, A.H. Jafari, *Corrosion*, 68 (2012) 600.
16. H. Zarrok, S.S. Al-Deyab, A. Zarrouk, R. Salghi, B. Hammouti, H. Oudda, M. Bouachrine, F. Bentiss, *Int. J. Electrochem. Sci.*, 7 (2012) 4047.
17. Zarrouk, B. Hammouti, H. Zarrok, M. Bouachrine, K.F. Khaled, S.S. Al-Deyab, *Int. J. Electrochem. Sci.* 7 (2012) 89.

18. A. Zarrouk, B. Hammouti, A. Dafali, H. Zarrok, R. Touzani, M. Bouachrine, M. Zertoubi, *Res. Chem. Intermed.*,, 38 (2012) 1079.
19. F. Bentiss, C. Jama, B. Mernari, H. El Attari, L. El Kadi, M. Lebrini, M. Traisnel, M. Lagrenee, *Corros. Sci.*, 51 (2009) 1628.
20. T.K. Dong, A. Kirchev, F. Mattera, J. Kowal, Y. Bultel, *J. Electrochem. Soc.*, 158 (2011) A326.
21. K. Laarej, M. Bouachrine, S. Radi, S. Kertit, B. Hammouti, *E-Journal of Chemistry*, 7 (2010) 419.
22. K. Barouni, L. Bazzi, R. Salghi, M. Mihit, B. Hammouti, A. Albourine, S. El Issami, *Mater. Let.*, 62 (2008) 3325.
23. A. Chetouani, M. Daoudi, B. Hammouti, T. Ben Hadda, M. Benkaddour, *Corros. Sci.*, 48 (2006) 2987.
24. M. Bouklah, A. Attayibat, S. Kertit, A. Ramdani, B. Hammouti, *Applied Surface Science*, 242 (2005) 399.
25. N. Boussalah, S. Ghalem, S. El Kadiri, B. Hammouti, R. Touzani, *Res. Chem. Intermed.*, 38 (2012) 2009.
26. S.M.A. Hosseini, M.J. Bahrami, A. Dorehgiraee, *Mater. Corros.-Werkst. Korros.*, 63 (2012) 627.
27. A.D. Xie, L.L. Zhou, W. Ruan, D.L. Wu, W.L. Luo, *Acta Physica Sinica*, 61 (2012) art N° 043302.
28. A. Zarrouk, H. Zarrok, R. Salghi, B. Hammouti, S.S. Al-Deyab, R. Touzani, M. Bouachrine, I. Warad, T.B. Hadda, *Int. J. Electrochem. Sci.*, 7 (2012) 6353.
29. K.F. Khaled, *Corros. Sci.*, 53 (2011) 3457.
30. A. Yurt, G. Bereket, C. Ogretir, *J. Mol. Struc.-Theochem*, 725 (2005) 215.
31. F. Bentiss, M. Lebrini, N.E. Chihib, M. Abdalah, C. Jama, M. Lagrenee, S.S. Al-Deyab, B. Hammouti, *Int. J. Electrochem. Sci.*, 7 (2012) 3947.
32. H. Zarrok, A. Zarrouk, B. Hammouti, R. Salghi, C. Jama, F. Bentiss, *Corros. Sci.*, 64 (2012) 243.
33. B.S. Sanatkumar, J. Nayak, A.N. Shetty, *Chem. Eng. Comm.*, 199 (2012) 1610.
34. A.K. Singh, E.E. Ebenso, M.A. Quraishi, *Int. J. Electrochem. Sci.*, 7 (2012) 2320.
35. L. Afia, R. Salghi, E.H. Bazzi, A. Zarrouk, B. Hammouti, M. Bouri, H. Zarrouk, L. Bazzi, L. Bammou, *Res. Chem. Intermed.*, 38 (2012) 1707.
36. H. Akrout, L. Bousselmi, S. Maximovitch, E. Triki, F. Dalard, *J. Mater. Sci.*, 47 (2012) 8085.
37. A.M. Al-Sabagh, M.A. Migahed, M. Abd El-Raouf, *Chem. Eng. Comm.*, 199 (2012) 737.
38. R. Baskar, M. Gopiraman, D. Kesavan, I.S. Kim, K. Subramanian, *Ind. Eng. Chem. Res.*, 51 (2012) 3966.
39. D. Ben Hmamou, R. Salghi, L. Bazzi, B. Hammouti, S.S. Al-Deyab, L. Bammou, A. Bouyanzer, *Int. J. Electrochem. Sci.*, 7 (2012) 1303.
40. K. Cao, W.H. Li, L.M. Yu, *Int. J. Electrochem. Sci.*, 7 (2012) 806.
41. M. Zunita, D. Wahyuningrum, Buchari, B. Bundjali, *Int. J. Electrochem. Sci.*, 7 (2012) 3274.
42. F. Branzoi, V. Branzoi, I. Harabor, *Revista De Chimie*, 62 (2011) 1090.
43. G. Mayakrishnan, S. Pitchai, K. Raman, A.R. Vincent, S. Nagarajan, *Ionics*, 17 (2011) 843.
44. M. Vishnudevan, *E-Journal of Chemistry*, 8 (2011) S53.
45. A.Y. Musa, A.A.H. Kadhum, M.S. Takriff, A.R. Daud, S.K. Kamarudin, N. Muhamad, *Corro. Eng. Sci. Techn.*, 45 (2010) 163.
46. K. Benbouya, B. Zerga, M. Sfaira, M. Taleb, M.E. Touhami, B. Hammouti, H. Benzeid, E.M. Essassi, *Int. J. Electrochem. Sci.* 7 (2012) 6313.
47. P. Thiraviyam, K. Kannan, P. Premkumar, *J. Chem.* (2013).
48. M. Abdallah, I. Zaafarany, J.H. Al-Fahemi, Y. Abdallah, A.S. Fouda, *Int. J. Electrochem. Sci.* 7 (2012) 6622.
49. H. Zarrok, A. Zarrouk, R. Salghi, Y. Ramli, B. Hammouti, S.S. Al-Deyab, E.M. Essassi, H. Oudda, *Int. J. Electrochem. Sci.*, 7 (2012) 8958.
50. R. Arefinia, A. Shojaei, H. Shariatpanahi, J. Neshati, *Prog. Org. Coat.*, 75 (2012) 502.
51. J. Halambek, K. Berkovic, *Int. J. Electrochem. Sci.*, 7 (2012) 8356.
52. F.B. Ravari, A. Dadgarinezhad, *Prot. Met. Phys. Chem. Surf.*, 48 (2012) 265.

53. V.E. Selvi, H. Seenivasan, K.S. Rajam, *Surf. Coat. Techn.*, 206 (2012) 2199.
54. A. Chetouani, B. Hammouti, *Bull. Electrochem.*, 19 (2003) 23.
55. A. Chetouani, A. Aouniti, B. Hammouti, N. Benchat, T. Benhadda, S. Kertit, *Corros. Sci.*, 45 (2003) 1675.
56. A. Chetouani, K. Medjahed, K.E. Benabadji, B. Hammouti, S. Kertit, A. Mansri, *Prog. Org. Coat.*,, 46 (2003) 312.
57. A. Chetouani, B. Hammouti, A. Aouniti, N. Benchat, T. Benhadda, *Prog. Org. Coat.*, 45 (2002) 373.
58. M. Benabdellah, A. Yahyi, A. Dafali, A. Aouniti, B. Hammouti, A. Ettouhami, *Arab. J. Chem.*, 4 (2011) 243.
59. M. Gopiraman, N. Selvakumaran, D. Kesavan, I.S. Kim, R. Karvembu, *Ind. Eng. Chem. Res.*, 51 (2012) 7910.
60. B. Joseph, M. Prajila, A. Joseph, *J. Disp. Sci. Techn.*, 33 (2012) 739.
61. A.Y. Musa, A.B. Mohamad, M.S. Takriff, R.T.T. Jalgham, *Res. Chem. Intermed.*, 38 (2012) 453.
62. P.M. Niamien, F.K. Essy, A. Trokourey, A. Yapi, H.K. Aka, D. Diabate, *Mat. Chem. Phys.*, 136 (2012) 59.
63. Z. El Adnani, M. McHarfi, M. Sfaira, A.T. Benjelloun, M. Benzakour, M.E. Touhami, B. Hammouti, M. Taleb, *Int. J. Electrochem. Sci.*, 7 (2012) 3982.
64. A.S. Fouda, M. Abdallah, I.S. Ahmed, M. Eissa, *Arab. J. Chem.*, 5 (2012) 297.